Journal of Hydroscience and Hydraulic Engineering
Vol. 16, No. 2, November, 1998, 35-48

A Numerical Study on a Cold Air Flow Causing the Formation of Snow Clouds over Sapporo City

By

Keisuke Nakayama

Research Associate, Hydraulic Engineering,
Hokkaido University, Sapporo, Japan

Kazuhiko Nakajima

Water Resauces Development Public Coorporation,
Iyomishima city, Japan

Kazuyoshi Hasegawa

Research Associate, Department of Civil Engineering,
Hokkaido University, Sapporo, Japan

and

Mutsuhiro Fujita

Professor, Department of Civil Engineering,
Hokkaido University, Sapporo, Japan

SYNOPSIS

In this study, we simulated a cold air flow occurring near the land surface in winter, and we compared with an actual cold air flow that occurred over Ishikari Bay on Feb. 17-18, 1996. It was assumed that a cold air is caused by the radiative cooling effect and that a cold air flow behaves like a density current. A cold air flow equation that takes into account bouyancy effects was used to predict the cold air flow. Kytoon observations showed the formation of a cold air flow extending to Ishikari Bay at 6:00 a.m. on Feb. 18. Numerical calculation result indicates that the calculated cold air flow causing the formation of snow clouds by an ascend wind agreed with the observed one at 6:00. It was also found that the friction coefficient between a cold air flow and a monsoon, and an upper wind are important for predicting the occurrence of an extended cold air flow.

INTRODUCTION

In winter, various types of snow clouds occur around Ishikari Bay, causing heavy snowfall. One frequently occurring pattern is the formation of snow clouds accompanying a cold air flow. On a mountain slope, cold air occurs due to radiative cooling, and it flows down the mountain slope due to gravity, behaving like a density current. When a cold air flow extends over Ishikari Bay, it behaves like a weather front, and snow clouds are formed due to the ascending wind at the tip of the front. These snow clouds move over Ishikari Plain, causing heavy snowfall. Therefore, it is necessary to predict the occurence of such snow clouds. However, predicting the occurence of such clouds is difficult because the cold air flow caused by radiative cooling must first be predicted.

Many studies have been reported about cold air flows as follows; a study on cold air flows around Ishikari river watershed with consideration to the relationship between snow fall and pressure patterns[1]; a study on a cold air flow observed by Kytoon[2]; experimental studies on a density current[3][4][5]; and a study on snow clouds

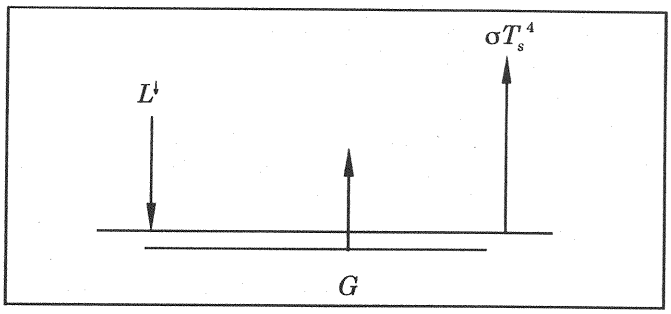

Fig. 1 Model of heat balance during the night

accompanying a cold air flow from doppler radar data[6]. These studies have provided much useful information on cold air flows but not sufficient information for predicting a cold air flow.

Therefore, in this study, we propose equations, which were used to predict a cold air flow that occurred on Feb 17-18, 1996, for predicting a cold air flow.

COLD AIR BY RADIATIVE COOLING

Radiative cooling theory

The theory of radiative cooling was given by Kondoh[7][8][9][10]. Fig. 1 shows the heat balance during night. Eq.(1) is a heat balance equation,

$$L^{\downarrow} = \sigma T_S^4 - G, \tag{1}$$

where $L^{\downarrow}$=long-wave radiative heat flux from the atomosphere, G=conduction heat flux underground, σT_s^4=long-wave radiative heat flux from the ground, and σ=stephan boltzmann constant.

During the night, $L^{\downarrow}$ is approximately equal to the long-wave radiative heat flux from the atomosphere in the evening. Therefore, net radiative heat flux in the evening is obtained as Eq.(2).

$$Rn_0 = \sigma T_S^4 - L_0^{\downarrow}, \tag{2}$$

where $L_0^{\downarrow}$=long wave radiative heat flux from the atomosphere in the evening, and Rn_0=net radiative heat flux.

We can obtain a maximum temperature fall as Eq.(3) when net radiative heat flux is equal to 0. Then the maximum temperature fall is obtained by Eq.(4).

$$T_{RAD} = \left(\frac{L_0^{\downarrow}}{\sigma}\right)^{\frac{1}{4}} \tag{3}$$

$$DT_{\max} = T_0 - T_{RAD}, \tag{4}$$

where T_{RAD}=extreme temperature, and $DT_{\max}$=maximum temperature fall.

The long-wave radiative heat flux is obtained by Kondoh's equation[10]:

$$L_0^{\downarrow} = (0.74 + 0.19x + 0.07x^2)\sigma T_0^4 \tag{5}$$

$$x = \log_{10} \omega_{TOP}^{*},$$

where ω^*_{TOP}=effective vapor pressure.

Effective vapor pressure is obtained by Eq.(6).

$$\omega_{TOP}^{*} = \sum_{n=0}^{\infty} \left\{ -\frac{0.622}{g} \int_{P_n}^{P_{n+1}} \frac{e}{P - 0.378e} \left(\frac{P}{P_0}\right) dP \right\}, \tag{6}$$

where g=gravity accelaration, P_0=pressure at the surface, P_0=1013hPa, and e=water vapor pressure.

Water vapor pressure is obtained by Clausius-Clapeyron's equation:

$$\frac{1}{e_{SAT}}\frac{de_{SAT}}{dT}=\frac{l}{RwT^2}, \tag{7}$$

where a=7.5 and b=237.3 on water, a=9.5 and b=262.3 on ice, and T=temperature.

Eq.(8) shows the saturated water vapor pressure equation by Tetens.

$$e_{SAT}=6.11\times 10^{aT/(b+T)}, \tag{8}$$

where l=latent heat of waporization, and Rw=the specific gas constant of water vapor.

In order to obtain the vertical temperature profile, which is ralated to a cold air, in the atmosphere near the surface an equation of heat conduction (Eq.(9)) is used:

$$\frac{\partial T_{(z,t)}}{\partial t}=\frac{\lambda_G}{C_\rho}\frac{\partial^2 T}{\partial z^2}, \tag{9}$$

where C_ρ=heat capacity, and λ_G=coefficient of thermal conductivity.

The initial condition and boundary condition are given as Eq.(10) and Eq.(11), respectively:

$$T(z,0)=T_0 \tag{10}$$

$$\lambda_G\left(\frac{\partial T}{\partial z}\right)_{z=0}=Rn_0-f(T_0-T_{(0,t)}) \tag{11}$$

$$f=4\sigma T_0^3.$$

Eq.(9) and Eq.(11) are transformed into Eq.(13) and Eq.(14) by using Laplace transformation:

$$sL\left[T_{(z,t)}\right]-T_0=\frac{\lambda_G}{C_\rho}L\left[\frac{\partial^2 T_{(z,t)}}{\partial z}\right] \tag{12}$$

$$\theta=\frac{T_0}{s}+ce^{-z\sqrt{\frac{C_\rho}{\lambda_G}s}} \tag{13}$$

$$\lambda\left(\frac{\partial\theta}{\partial z}\right)_{z=0}=\frac{Rn_0}{s}-\frac{fT_0}{s}+f\theta. \tag{14}$$

c is derived from Eq.(14) and Eq.(13) is transformed into Eq.(16), from which Eq.(17) is obtained.

$$c=\frac{-Rn_0}{s\left(\sqrt{C_\rho\lambda_G s}+f\right)} \tag{15}$$

$$\theta=\frac{T_0}{s}-\frac{Rn}{f}\frac{\left(\frac{f}{\sqrt{C_\rho\lambda_G}}\right)}{\left\{s\left(\sqrt{s}+\frac{f}{\sqrt{C_\rho\lambda_G}}\right)\right\}}e^{-z\sqrt{\frac{C_\rho}{\lambda_G}s}} \tag{16}$$

$$T_{(z,t)}=T_0-\frac{Rn_0}{f}\left\{1-Exp\left(\frac{f}{\lambda_G}z+\frac{f^2t}{C_\rho\lambda_G}\right)\times Erfc\left(\frac{z}{2}\sqrt{\frac{C_\rho}{t\lambda_G}}+f\sqrt{\frac{t}{C_\rho\lambda_G}}\right)\right. \tag{17}$$

$$Erfc(\gamma)=1-\frac{2}{\sqrt{\pi}}\int_0^\gamma Exp(-\gamma^2)d\gamma.$$

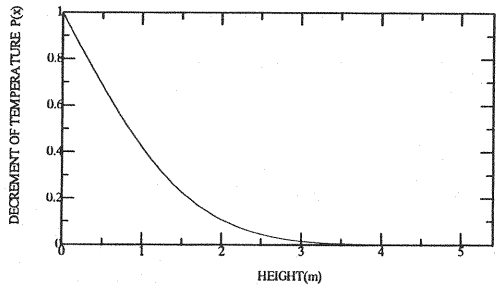

Fig. 2 Rate of temperature fall 10 hours after the beginning of radiative cooling

Eq.(18) is obtained when z=0.

$$T_0 - T_S = DT_{\max} \times P(x) \tag{18}$$

$$P(x) = 1 - Exp(x)Erfc\left(\sqrt{x}\right)$$

$$x = \frac{f^2 t}{C_\rho \lambda_G} = \frac{(4\sigma T_0^3)^2 t}{C_\rho \lambda_G} .$$

Generation intensity of cold air

The profile of vertical temperature in the atmosphere is obtained by Eq. (18). However, in this section we solve Eq.(9) again by using the initial and the boundary conditions (Eq.(20)), because it is too difficult to obtain the generation intensity of cold air from Eq.(18), and Eq.(20) also gives the same solution comparing with Eq.(10) and Eq.(11).

$$\frac{\partial T_{(z,t)}}{\partial t} = \frac{\lambda}{C}\frac{\partial^2 T}{\partial z^2} \tag{19}$$

$$\begin{cases} T_{(0,t)} = T_0 \\ T_{(z,0)} = 0 \end{cases} . \tag{20}$$

Eq.(21) is obtained by using Laplace transformation.

$$\frac{\partial^2 F}{\partial z^2} - \frac{C}{\lambda} sF = 0 \tag{21}$$

$$F = C1\exp\left(-\sqrt{\frac{C}{\lambda}sz}\right) . \tag{22}$$

Eq.(24) is obtained from using Eq.(23), which is transformed from Eq.(20).

$$F\big|_{Z=0} = \frac{T_0}{s} \tag{23}$$

$$F = \frac{T_0}{s}\exp\left(-\sqrt{\frac{C}{\lambda}sz}\right) . \tag{24}$$

Eq.(25) and Eq.(26) are obtained from Eq.(24).

$$T_{(x)} = T_0 Erfc(x) \tag{25}$$

$$x = \frac{1}{2}\sqrt{\frac{C}{\lambda t}}z . \tag{26}$$

Fig. 2 shows the vertical temperature fall rate profile that is 10 hours after the beginning of radiative cooling when the coefficient of thermal conductivity = 0.025 $Wm^{-1}K^{-1}$ and heat capacity = 0.0012×10^{6} $Jm^{-3}K^{-1}$. Ten percent of the temperature fall occurs at a height of 2 m. When a cold air flow extends over Ishikari bay, the velocity of Monsoon at a high altitude is smaller than usual. Therefore, sensible heat flux is small and does not have to be considered in this phenomenon.

If the effective height of radiative cooling in Eq.(26) is lower than the height at which the temperature fall rate is 10 percent, the generated cold air height can be obtained from Eq.(27).

$$z = 2\sqrt{\frac{\lambda}{C}t} \quad . \tag{27}$$

Therefore, the intensity of a cold air generation (Eq.(28)) is obtained by differentiating Eq.(27).

$$\frac{\partial z}{\partial t} = \sqrt{\frac{\lambda}{Ct}} \quad . \tag{28}$$

COLD AIR FLOW EQUATION

It was assumed that cold air flow behaves like a density current. Therefore, Eqs.(29)-(32) are proposed. Eqs.(29), (30) and (31) are kinetic energy equations in the x, y and z directions, respectively. Eq.(32) is a conservation equation. In Eq.(29) and (30), the 3rd and 4th terms are the Coriolis force and the friction, which is expalained in the next section, of the interface between a cold air flow and the upper air, respectively. Eq.(31) is obtained under hydrostatic considering only bouyancy effect. In these equations, Boussinesq approximation is assumed:

$$\begin{cases} \dfrac{\partial uh}{\partial t} + \dfrac{\partial uuh}{\partial x} + \dfrac{\partial vuh}{\partial y} - fvh + f_i(u-U)|u-U| = -\dfrac{1}{\rho_T}\displaystyle\int_0^h \left(\frac{\partial p}{\partial x}\right)dz + h\nu\nabla^2 u & (29) \\ \dfrac{\partial vh}{\partial t} + \dfrac{\partial uvh}{\partial x} + \dfrac{\partial vvh}{\partial y} + fuh + f_i(v-V)|v-V| = -\dfrac{1}{\rho_T}\displaystyle\int_0^h \left(\frac{\partial p}{\partial y}\right)dz + h\nu\nabla^2 v & (30) \\ 0 = -\dfrac{1}{\rho_T}\dfrac{\partial p}{\partial z} - g + \alpha g(T - T_T) & (31) \\ \dfrac{\partial h}{\partial t} + \dfrac{\partial uh}{\partial x} + \dfrac{\partial vh}{\partial y} = R \quad , & (32) \end{cases}$$

where h=cold air flow height, u and v=velocity components in the x and y directions, respectively, f=Coriolis coefficient, f_i=friction coefficient of the interface of the two-phase flow, ρ_T=density of a cold air flow, ρ=density of the upper air, T_T=temperature of a cold air flow, T=temperature which is changed by radiative cooling, and R=intensity of a cold air genaration.

Eq.(33) is obtained by integrating Eq.(31). Eq.(34) and Eq.(35) are obtained by substituting Eq.(33) into Eq.(29) and Eq.(30), respectively.

$$\begin{aligned} &\frac{\partial p}{\partial z} = \rho_T g\left(1 + \alpha(T - T_T)\right) \\ &p = \rho g(H - Z - h) + \rho_T g\left(1 + \alpha(T - T_T)\right)h + \rho_T gZ - \rho_T gz \qquad (33) \\ &\begin{cases} \dfrac{\partial p}{\partial x} = (\rho_T - \rho)g\dfrac{\partial h}{\partial x} + \alpha(T - T_T)g\dfrac{\partial h}{\partial x} + (\rho_T - \rho)g\dfrac{\partial Z}{\partial x} \\ \dfrac{\partial p}{\partial y} = (\rho_T - \rho)g\dfrac{\partial h}{\partial y} + \alpha(T - T_T)g\dfrac{\partial h}{\partial y} + (\rho_T - \rho)g\dfrac{\partial Z}{\partial y} \end{cases} \\ &\int_0^h \left(\frac{\partial p}{\partial x}\right)dz = (\rho_T - \rho)gh\frac{\partial h}{\partial x} + \alpha(T - T_T)gh\frac{\partial h}{\partial x} + (\rho_T - \rho)gh\frac{\partial Z}{\partial x} \end{aligned}$$

$$\int_0^h \left(\frac{\partial p}{\partial x}\right) dz = (\rho_T - \rho) gh \frac{\partial h}{\partial y} + \alpha (T - T_T) gh \frac{\partial h}{\partial y} + (\rho_T - \rho) gh \frac{\partial Z}{\partial y}$$

$$\frac{\partial uh}{\partial t} + \frac{\partial uuh}{\partial x} + \frac{\partial vuh}{\partial y} - fvh + f(u-U)|u-U| =$$

$$-\varepsilon gh \frac{\partial h}{\partial x} + \frac{\alpha (T - T_T)}{\rho_T} gh \frac{\partial h}{\partial x} - \varepsilon gh \frac{\partial Z}{\partial x} + h\nu \nabla^2 u \qquad (34)$$

$$\frac{\partial vh}{\partial t} + \frac{\partial uvh}{\partial x} + \frac{\partial vvh}{\partial y} + fuh + f_i (v-V)|v-V| =$$

$$-\varepsilon gh \frac{\partial h}{\partial y} + \frac{\alpha (T - T_T)}{\rho_T} gh \frac{\partial h}{\partial y} - \varepsilon gh \frac{\partial Z}{\partial y} + h\nu \nabla^2 v \qquad (35)$$

$$\frac{\partial h}{\partial t} + \frac{\partial uh}{\partial x} + \frac{\partial vh}{\partial y} = R. \qquad (36)$$

Eqs.(34) to (36) are called cold air flow equations in this study.

In the numerical computation, finite difference is used. Eqs.(37)-(42) show the algorithm for calculation.

$$\begin{cases} \dfrac{\tilde{u} - u^n}{\Delta t} = -\left(u \dfrac{\partial u}{\partial x} + v \dfrac{\partial u}{\partial y} - fv + \dfrac{f_i}{h}(u-U)|u-U| + \dfrac{u}{h} R \right)^n \\ \qquad\qquad - \varepsilon g \dfrac{\partial (\tilde{h} + z)}{\partial x} + \left(\alpha (T - T_T) g \right)^n \dfrac{\partial (\tilde{h} + z)}{\partial x} \qquad (37) \\ \dfrac{\tilde{v} - v^n}{\Delta t} = -\left(u \dfrac{\partial v}{\partial x} + v \dfrac{\partial v}{\partial y} + fu + \dfrac{f_i}{h}(v-V)|v-V| + \dfrac{v}{h} R \right)^n \\ \qquad\qquad - \varepsilon g \dfrac{\partial (\tilde{h} + z)}{\partial y} + \left(\alpha (T - T_T) g \right)^n \dfrac{\partial (\tilde{h} + z)}{\partial y} \qquad (38) \end{cases}$$

$$\begin{cases} \dfrac{u^{n+1} - \tilde{u}}{\Delta t} = \nu \dfrac{\partial^2 \tilde{u}}{\partial x^2} + \nu \dfrac{\partial^2 \tilde{u}}{\partial y^2} \qquad (39) \\ \dfrac{v^{n+1} - \tilde{v}}{\Delta t} = \nu \dfrac{\partial^2 \tilde{v}}{\partial x^2} + \nu \dfrac{\partial^2 \tilde{v}}{\partial y^2} \qquad (40) \end{cases}$$

$$\frac{\tilde{h} - h^n}{\Delta t} + \tilde{u} \frac{\partial \tilde{h}}{\partial x} + \tilde{h} \frac{\partial \tilde{u}}{\partial x} + \tilde{v} \frac{\partial \tilde{h}}{\partial y} + \tilde{h} \frac{\partial \tilde{v}}{\partial y} = 0 \qquad (41)$$

$$\frac{h^{n+1} - \tilde{h}}{\Delta t} = R. \qquad (42)$$

THE FRICTION OF THE INTERFACE OF THE TWO-PHASE FLOW

Many experiments and observations have been carried out in past studies to obtain the friction of the interface of the two-phase flow. In this section, we present a new formula for estimating the friction coefficient of the interface by considering the Monin-Obukhov theory and turbulent separation theory.

The friction coefficient of the interface and Keulegan number

Fig. 3 shows the relationship between the friction coefficient of the interface and the Keulegan number. Black colored circle indicates $Re \leqq 2 \times 10^5$ and white circle

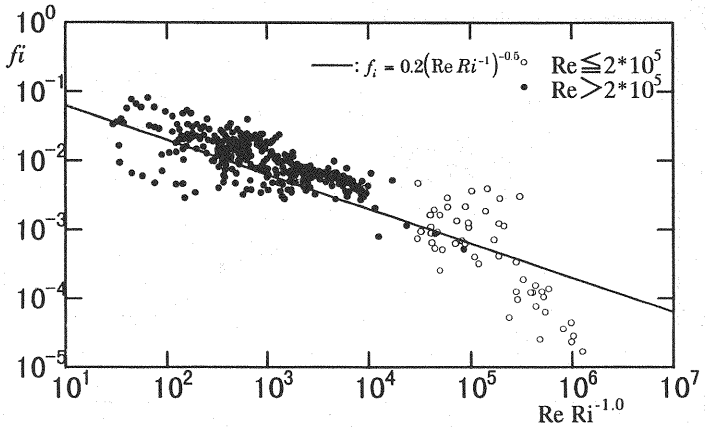

Fig. 3 Intefacial resistance coefficient and Keulegan number

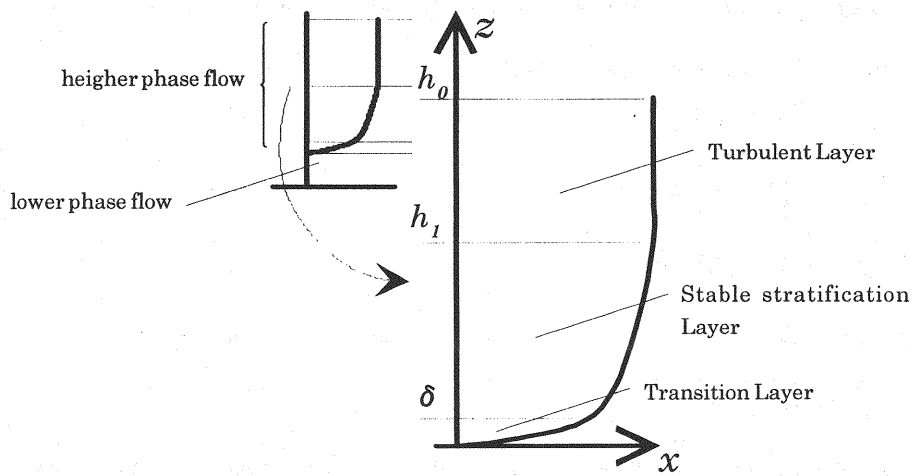

Fig. 4 Intefacial resistance coefficient and Keulegan number

indicates Re>2×10⁵. The solid line in Fig. 3 was calculated using a formula proposed by Kaneko[12]. However, the greater the Reynolds number is, the worse the agreement becomes. As turbulent separation can occur at a greater Reynolds number there though to be two tendencies of the interfacial resistance coefficient in Fig. 3. Therefore, in this study two formulae (Re≦2×10⁵ and Re>2×10⁵) were used.

At Re≦2×10⁵, Linear+Log law was used to determine the velocity and the friction coefficient of the interface of the two-phase flow. Fig. 4 shows the model velocity profile for a two-phase flow. In the lower phase, velocity is neglected because it is much smaller than the upper flow one. In each layer, the velocity profiles are obtained from Eq.(45), Eq.(47) and Eq.(48), respectively.

・Transition Layer $z \leqq \delta$

$$\delta = \frac{R_\delta \nu}{u_*} \tag{43}$$

$$\mu \frac{\partial u}{\partial z} = \rho u_*^2 \tag{44}$$

$$u = \frac{u_*^2}{\nu} z \quad \left(\because u|_{z=0} = 0\right). \tag{45}$$

where δ=transition layer height, R_δ=11.6, u_*=friction velocity, ν=viscosity, and β=4~7.

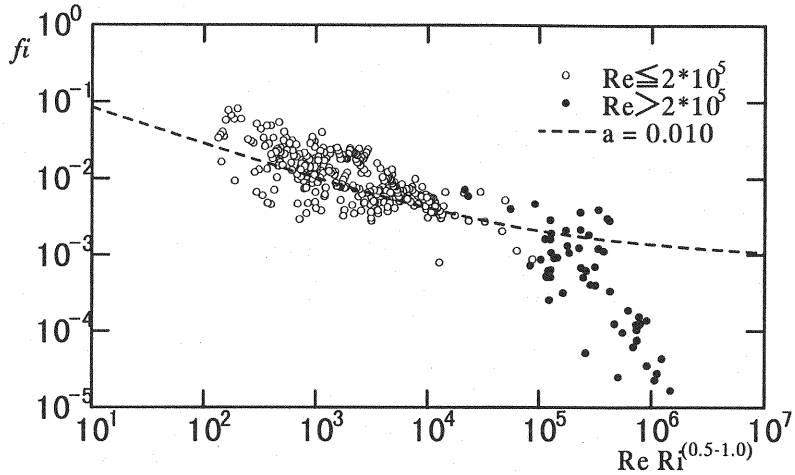

Fig. 5 Intefacial resistance coefficient and Eq. 56 (a=0.010,0.002,b=0.5)

· Stable stratification Layer $\delta \leqq z \leqq h_1$

$$\frac{\partial u}{\partial z} = \frac{u_*}{\kappa z}\left(1+\beta\frac{z}{L}\right) \tag{46}$$

$$\frac{u}{u_*} = \frac{1}{\kappa}\left(\ln z + \frac{\beta}{L}z\right) + c_1 \tag{47}$$

· Turbulent Layer $h_1 \leqq z \leqq h_0$

$$u = u_0\ , \tag{48}$$

Eq.(45) is equal to Eq.(47) when z=δ, and Eq.(49) is derived.

$$\frac{u}{u_*} = \frac{1}{\kappa}\left(\ln\frac{z}{\delta} + \beta\frac{z-\delta}{L}\right) + \frac{u_*}{\nu}\delta\ . \tag{49}$$

Eq.(57) is obtained from Eq.(48). Eq.(50) is proposed in this study, and shows that the more stable the flow becomes, the more the turbulent heat flux decreases.

$$|\theta w| = -\Delta\theta u_0 a Ri^{-b} \tag{50}$$

$$Ri = \frac{\alpha\Delta\theta g h_0}{u_0^{\,2}} \tag{51}$$

$$\mathrm{Re} = \frac{u_0 h_0}{\nu} \tag{52}$$

$$f_i' = \left(\frac{u_*}{u_0}\right)^2,\ f_i = 2f_i' \tag{53}$$

$$h_1 = \beta_b L \quad (\beta_b = 2\sim 5) \tag{54}$$

$$L = -\frac{u_*^{\,3}}{\kappa g\alpha|\theta w|} = \frac{h_0 u_*^{\,3}}{a\kappa u_0^{\,3}} Ri^{b-1} \tag{55}$$

$$\frac{\delta}{L} = \frac{a\kappa R_\delta}{f_i^2} \times \frac{1}{\mathrm{Re}\,Ri^{b-1}} \tag{56}$$

$$1 = \frac{\sqrt{f_i}}{\kappa}\ln\frac{\beta_b f_i'^{\,2}}{a\kappa R_\delta}\mathrm{Re}\,Ri^{b-1} + \frac{\beta}{\kappa}\beta_b\sqrt{f_i'} - \frac{\beta_b a R_\delta}{f_i'^{\,3/2}} \times \frac{1}{\mathrm{Re}\,Ri^{b-1}} + R_\delta\sqrt{f_i'}\ . \tag{57}$$

It was found that the friction coefficient of the interface is a function of $\mathrm{Re}Ri^{b-1}$. $\mathrm{Re}Ri^{b-1}$ is equal to the Keulegan number when b=0. However, turbulent heat flux

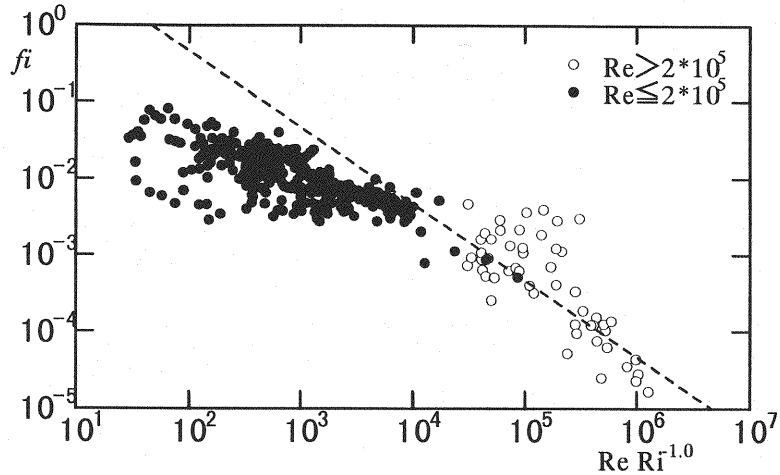

Fig. 6 Intefacial resistance coefficient and Eq. 61 (β=2)

is thought to be qualitatively changed by the stability and b is greater than 0. So in this study we used b=0.5 in Eq.(57).

The broken line in Fig. 5 shows the results calculated by Eq.(57). At Re$\leqq 2\times10^5$, the calculated results agree with the experimental and observed results.

At Re$>2\times10^5$, the Monin-Obukhov length is much smaller than the transition layer height. Therefore, a universal function such as Eq.(58) is used. The friction coefficient of the interface is obtained from Eq.(62) assuming that turbulent heat flux is given by Eq.(60). Eq.(62) shows that the friction coefficient is a function of the Keulegan number.

$$\frac{z}{L} \gg 1 \quad \frac{\kappa z}{u_*}\frac{\partial u}{\partial z} \sim \frac{z}{L} \tag{58}$$

$$u = \frac{u_*\beta}{\kappa L} z \tag{59}$$

$$|\theta w| = -\Delta\theta u_* \tag{60}$$

$$L = \frac{u_*^3}{\kappa g \alpha \Delta\theta u_*} \tag{61}$$

$$f_i = \frac{2\beta R_\delta}{\mathrm{Re}\, Ri^{-1}} . \tag{62}$$

The broken line in Fig. 6 shows the results calculated by Eq.(62). At Re$>2\times10^5$, the calculated results agree with the experimental and observed results.

RESULTS OF NUMERICAL SIMULATION

Numerical calculation

On the night of Feb. 18, 1996, a cold air flow was observed. Fig.7 shows the vertical temperature profile from 0:00 a.m. to 8:00 a.m. at the mouth of Ishikari River, based on Kytoon observations. At 6:00 a.m., temperature near the surface was lowest and the difference between the surface and that higher up was the greatest, indicating the occurrence of a cold air flow. Fig. 8 shows the vertical profile of the horizontal wind velocity at 6:00 am observed by Doppler Sodar. A shear layer was indicated at a height of 50 m. The thickness of the shear layer was about 1~10 m. Therefore, the viscosity is estimated to be 0.02 m^2/sec, and we used Eq.(62) to determine the friction coefficient of the interface.

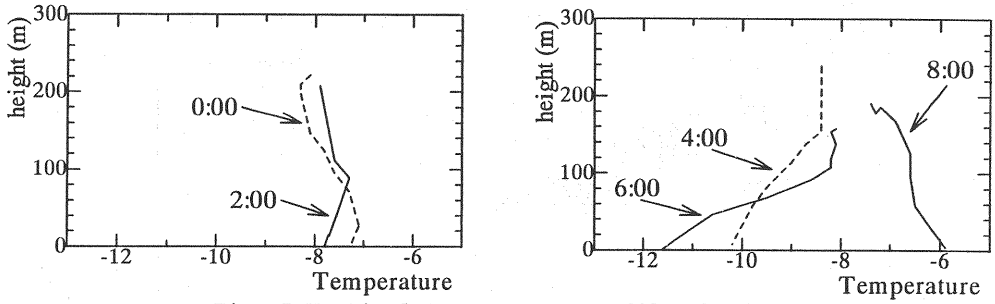

Fig. 7 Vertical temperature profile obtained from Kite balloon observations on Feb. 18, 1996

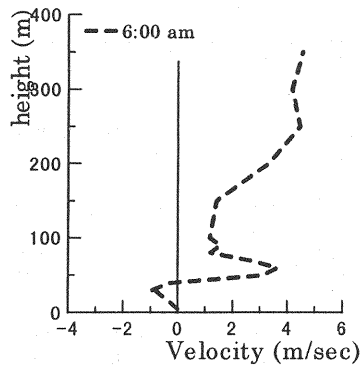

Fig. 8 Vertical profile of the horizontal wind velocity at 6:00 am

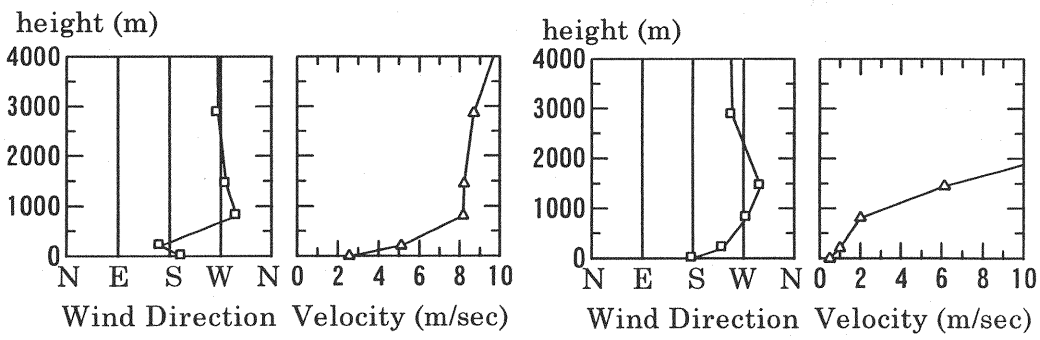

Fig. 9 Velocity profile obtained from Radio-sonde at 9:00 p.m. on Feb. 17 and at 9:00 a.m. on Feb. 18

Fig. 9 shows the velocity profile obtained from Radio-sonde data at 9:00 p.m. on Feb. 17 and at 9:00 a.m. on Feb. 18. Monsoon velocity is obtained by Fig. 9 and the intensity of a cold air generation is also obtained by using Radio-sonde data.

Fig. 10 shows the calculation area and the results of simulation at 2~12 hours after the beginning of the radiative cooling. After 2 hours, a cold air flow from Yoichi River extended over Ishikari bay and the cold air flow from Hamamasu river is suppressed because the Monsoon direction is west-northwest. After 4~8 hours, the cold air was accumulated around the south area of the mouth of Hamamasu River. After 10 hours, the cold air is accumulated greater; The cold air moved south and made a front, located 20 km from the mouth of Ishikari River.

The calculations show that Yoichi River and Hamamasu River have a great effect on the formation of the cold air flow front, and after the cold air is accumulated by the topography effect, it moves by the upper wind and it is strengthened.

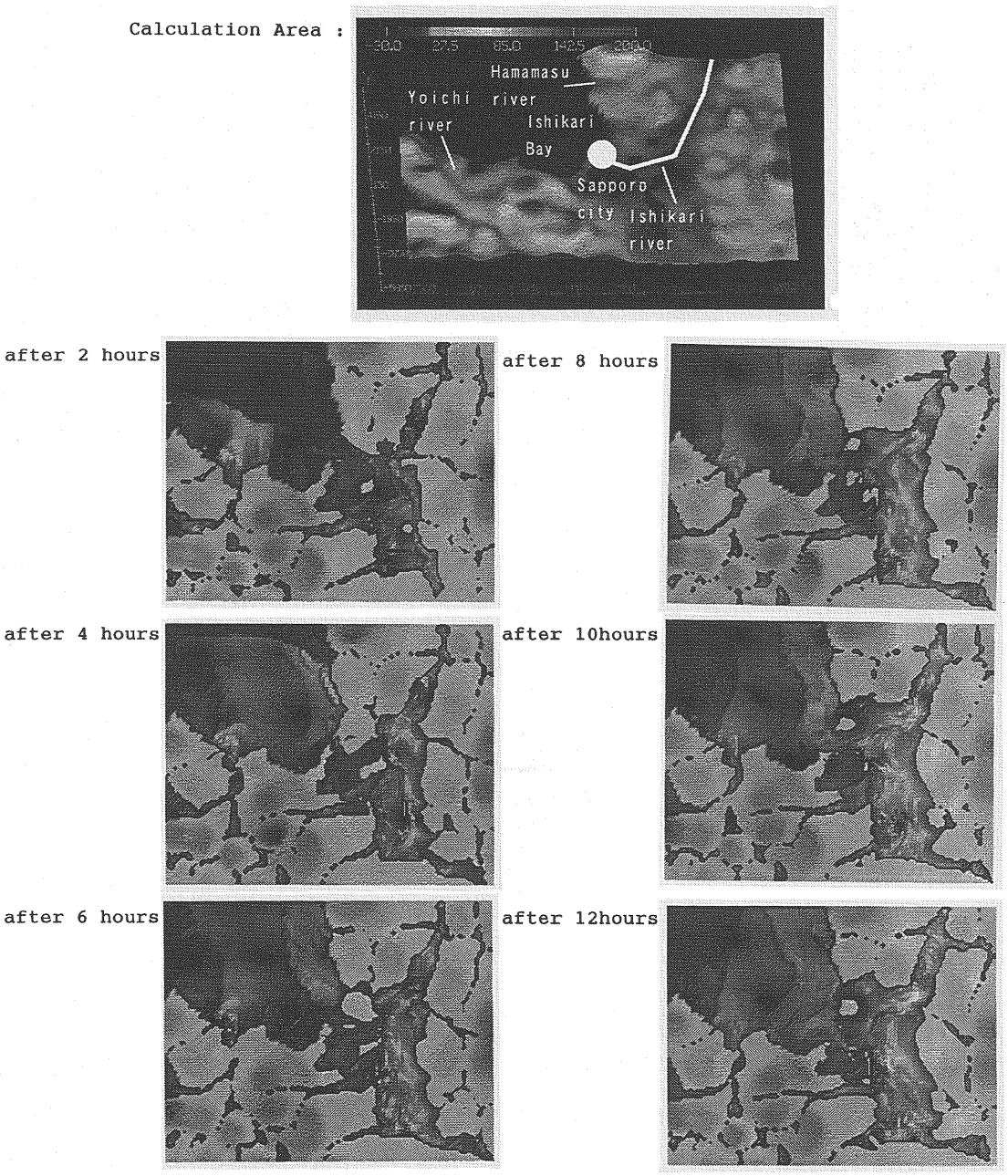

Fig. 10 Bird's-eye view of the calculation area
and numerically calculated cold air flow heights from 2 to 12 hours later

A comparison of simulation and observation results

Fig. 11 shows the wind vector in a cold air flow by numerical simulation and the observed wind vector at the surface by SNET (Sapporo information NETwork) at 6:00 a.m. on Feb. 18, 1996. In the left and right sides of Fig. 11(center), a cold air flow runs off the mountain slope and extends over Ishikari Bay. The results in Fig. 11(right) agrees with the observed results.

Fig. 12 shows the cold air height obtained by numerical simulation (left) and radar data by radar observation (right) at 6:00 a.m. on Feb. 18, 1996. When a cold air

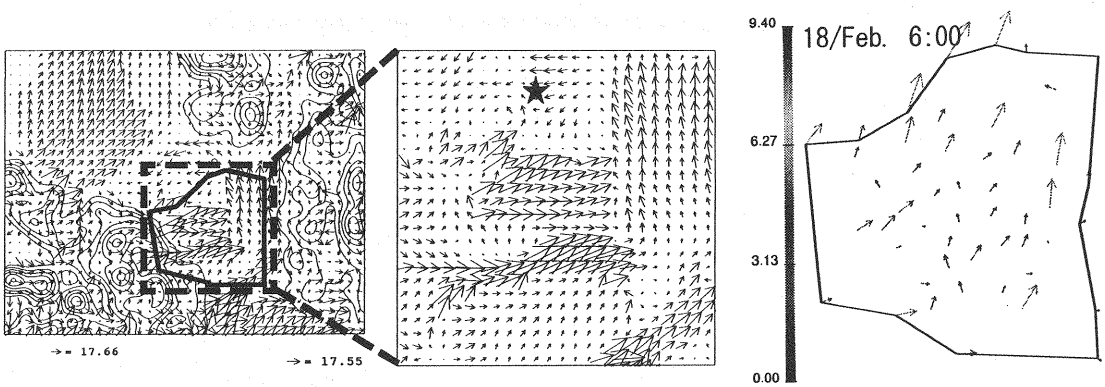

Fig. 11 At 6:00 a.m. on Feb. 18, 1996
wind vector according to numerical simulation (left and center) in a cold air flow
and wind vector according to surface observation (SNET) (right)

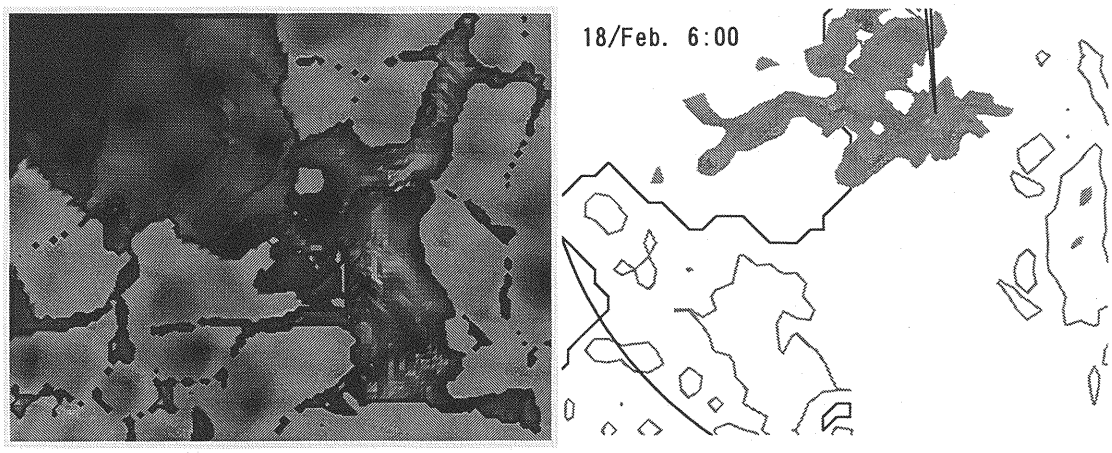

Fig. 12 At 6:00 a.m. on Feb. 18, 1996
cold air flow height obtained by numerical simulation (left)
and radar data by radar observation (right)

flow extends over Ishikari Bay, snow clouds form at the front of the cold air flow due to the ascending wind. The calculated location of the front of the cold air flow agrees with the location of the radar data. Fig. 12 shows that it does.

In Fig. 11, the star indicates the location of the Kite balloon and doppler sodar observation. At this point, the observed cold air flow height was about 60 m and the observed wind velocity was 2.6 m/sec. By numerical simulation, the height was 59.8m and the velocity was 3.1 m/sec. Thus, the observed and calculated values agree well.

CONCLUSIONS

(1) The intensity of a cold air genaration is derived theoretically by using radaitive cooling theory.

(2) A cold air flow equation was obtained by considering the buoyancy effect and the friction of the interface of two-phase flow. Hydrostatic is assumed, and this equation is vertically integrated. Therefore, it is easy to compute using this equation by finite difference.

(3) The front of a cold air flow that occurred at 6:00 a.m. on Feb. 18, 1996 was represented clearly by numerical simulation. The wind field, the location of the front, and the cold air height at the point of the Kite balloon observations agree well with the actual values.

REFFERNCES

1. Tatibana, Y.: SNOWFALLS AND THEIR RELATION TO COLD AIR DRAINAGE IN HOKKAIDO ISLAND,Institute of Low Temperature Science, Hokkaido University, January,11,1994
2. Berson.F.A.,: Some measurements on undercutting cold air, Quart. J. Royal Meteo. Soc., Vol.84, pp.1-16, 1958.
3. Simpson,J.E.,: A comparison between laboratory and atmospheric density currents, Quart. J. Royal Meteo. Soc., Vol.95,pp.758-765, 1969.
4. Britter,R.E., and J.E.SIMPSON,: Experiments on the dynamics of a gravity current head,J.Fluid Mech., vol.88, pp.223-240, 1978.
5. Simpson,J.E., and R.E.BRITTER,: The dynamics of the head of a gravity current advancing over a horizontal surface, J.Fluid Mech., vol.94, pp.477-495, 1979.
6. Tsuboki, K., Y. Fujiyoshi, and G. Wakahama,: Structure of a Land Breeze and Snowfall Enhancement at the Leading Edge, Journal of the Meteorological Society of Japan, pp.757-769, 1989.
7. Kondo,J., O.Kanechika, and N.Yasuda,: Heat and Momentum Transfers under Strong Stability in the Atmospheric Surface Layer, Journal of the atmospheric sciences, Vol.35, pp.1012-1021, 1978
8. Kondo,J. and Y.Mori; Analysis on nocturnal cooling at the regional meteorological stations Part 1., Tenki, No.29, vol.12, pp.1221-1233.
9. Kondo,J. and Y.Mori; Analysis on nocturnal cooling at the regional meteorological stations Part 2., Tenki, No.30, vol.3, pp.109-150.
10. Kondo,J. and H.Yamazawa; Nocturnal radiational cooling of the earth's surface with the snow-cover, and the extreme minimum air-temperature over Japan, Tenki, No.30, vol.6, pp.295-302.
11. Nakayama,K., K.Hasegawa and M.Fujita; Analysis of cold air flow with snow cloud in Ishikari bay, Journal of hydraulic, coastal and environmental engineering, No.539, pp.31-42.
12. Tamai,N., and T,Asaeda; A theory on the friction at the interaface of two-lyered flows, Journal of hydraulic, coastal and environmental engineering, JSCE, No.271, pp.67-81.
13. Nakayama,K., K.Hasegawa and M.Fujita; A study on the shape of a cold air flow around Ishikari bay in winter at a vertical plane, Annual journal of hydraulic engineering, JSCE, Vol.39, pp.177-182.
14. Nakayama, K., K. Hasegawa, M. Fujita, Characteristics of a Cold Air Flow in Winter with Consideration to the Influence from Topography, Proceedings of The First Korea-Japan Bilateral Seminar on Water Resources and Environment Research, pp.81-88, 20-23 August,1996.
15. Nakayama, K., K. Hasegawa, M. Fujita, Characteristics of Snow Clouds When a Cold Air Flow Appears Around Ishikari Bay, International Conference on Water Resources & Environment Research: Towards the 21th Century, 1996.

APPENDIX - NOTATION

The following symbols are used in this paper:

$L^{\downarrow}$	= long wave radiative heat flux from the atomosphere
G	= conduction heat flux underground
σT_s^4	= long wave radiative heat flux from the ground
σ	= stephan boltzmann constant
$L_0^{\downarrow}$	= long wave radiative heat flux from the atomosphere
Rn_0	= net radiative heat flux
T_{RAD}	= extreme temperature
$DT_{\max}$	= maximum temperature fall
ω^*_{TOP}	= effective vapor pressure
g	= gravity accelaration
P_0	= pressure at the surface
P_0	= 1013hPa
e	= water vapor pressure
l	= latent heat of vaporization
Rw	= the specific gas constant of watr vapor
C_ρ	= heat capacity
λ_G	= coefficient of thermal conductivity
h	= cold air flow height
u, v	= velocity component of x, y direction
f	= Coriolis coefficient
f_i	= interfacial resistance coefficient
ρ_T	= density of a cold air flow
ρ	= density of the upper air
θ_T	= temperature of a cold air flow
θ	= temperature which is changed by radiative cooling
R	= genaration intensity of a cold air
δ	= transition layer height
R_δ	= 11.6
u_*	= friction velocity
ν	= viscosity
β	= 4~7

(Received February 19, 1998; revised April 13, 1998)